First CoMFA Characterization of Vesamicol Analogs as Ligands for the Vesicular Acetylcholine Transporter

ARTICLE *in* JOURNAL OF MEDICINAL CHEMISTRY · MAY 2008

Impact Factor: 5.45 · DOI: 10.1021/jm700961r · Source: PubMed

5 AUTHORS, INCLUDING:

Barbara Wenzel
Helmholtz-Zentrum Dresden-Rossendorf
36 PUBLICATIONS **209** CITATIONS

First CoMFA Characterization of Vesamicol Analogs as Ligands for the Vesicular Acetylcholine Transporter

Andrzej Szymoszek,[†] Barbara Wenzel,[‡] Matthias Scheunemann,[‡] Jörg Steinbach,[‡] and Gerrit Schüürmann*[,†,§]

UFZ Department of Ecological Chemistry, Helmholtz Centre for Environmental Research, Permoserstr. 15, 04318 Leipzig, Germany, IIF Institute of Interdisciplinary Isotope Research, University of Leipzig, Permoserstr. 15, 04318 Leipzig, Germany, and Institute for Organic Chemistry, Technical University Bergakademie Freiberg, Leipziger Str. 29, 09596 Freiberg, Germany

Received August 2, 2007

Vesamicol derivatives are promising candidates as ligands for the vesicular acetylcholine transporter (VAChT) to enable in vivo imaging of cholinergic deficiencies if applied as positron emission tomography radiotracers. So far, optimization of the binding affinity of vesamicol-type ligands was hampered by the lack of respective quantitative structure–activity relationships. We developed the first quantitative model to predict, from molecular structure, the binding affinity of vesamicol-type ligands toward VAChT employing comparative molecular field analysis (CoMFA) for a set of 37 ligands, covering three different structural types (4-phenylpiperidine, spiro, and tropan derivatives of vesamicol). The prediction capability was assessed by leave-one-out cross-validation (LOO) and through leaving out and predicting 50% of the compounds selected such that both the training and the prediction sets cover almost the whole range of experimental data. The statistics indicate a significant prediction power of the models (q^2 (LOO) = 0.66, q^2 (50% out) = 0.59–0.74). The discussion includes detailed analyses of CoMFA regions critical for ligand−VAChT binding, identifying structural implications for high binding affinity.

Introduction

The cholinergic system in the brain is known to be involved in cognitive function and memory. Neurodegenerative disorders like Alzheimer's disease as well as physiological aging processes are characterized by a profound loss of central cholinergic neurons and resulting deficiencies in cholinergic neurotransmission.[1–4] The neurotransmitter acetylcholine, synthesized by the enzyme choline acetyltransferase in cholinergic presynaptic nerve terminals, is transported into synaptic vesicles by the vesicular acetylcholine transporter (VAChT[a]).[5] Located at the vesicle membrane, this binding protein contains 12 transmembrane domains and belongs to a family of transporters such as the vesicular monoamine transporters VMAT1 and VMAT2.[5–7] Besides other important constituent parts of the cholinergic system, for example, nicotinic acetylcholine receptors,[8] VAChT gained increasing interest in the last years as a target protein for in vivo imaging of cholinergic deficiencies using PET (positron emission tomography) or SPECT (single photon emission computed tomography).[9–11] Nowadays, PET is a routine method in modern nuclear medicine diagnostics, with fluorine-18 as the currently most widely used radionuclide,[12] mainly because of its imaging properties and its half-life (110 min), which is long enough to allow for an adequate distribution of the radiotracer. Therefore, ^{18}F-labeled radioligands with appropriate binding capacity for VAChT are highly promising candidates for a successful quantitative visualization of VAChT in cholinergic regions of the diseased brain.

The drug vesamicol, *trans*-2-(4-phenylpiperidino)cyclohexanol (see Figure 1), binds with considerable affinity (K_i = 7.6 nM,[13] corresponding to a free energy of binding of −46.3 kJ/mol at 25 °C) to an allosteric site in VAChT and inhibits the transport of acetylcholine noncompetitively.[14–17] However, vesamicol also demonstrates substantial affinity to sigma receptors, which are partly located in the same brain regions like VAChT.[13,18–20] Because of this low selectivity, vesamicol itself is not suitable for PET or SPECT imaging in brain. Therefore, in the past, numerous efforts have been undertaken to improve the VAChT selectivity by chemical modifications of the vesamicol structure. Most of the known compounds are structurally derived from benzovesamicol (ABV,[21] [^{18}F]NEFA,[22] [^{18}F]FEOBV,[23,24] [^{125}I]IBVM[25,26]) and trozamicol ([^{18}F]FBT[27–30] [$^{123/125}$I]MIBT;[31–33] see Figure 1). Although some of them were described as promising radiotracers based on their in vitro data or in vivo evaluation in rats, rodents, or nonhuman primates, only [^{123}I]IBVM and [^{18}F]NEFA were used for human neuroimaging studies in vivo.[34–36] Despite these attempts, none of the ligands synthesized so far has proven suitable for clinical application or for the purpose of brain imaging with PET.

Moreover, various vesamicol analogues have been synthesized with the goal to increase the binding affinity toward VAChT. While some ligands with stronger binding affinities have been found (see Table 3), there is still missing a quantitative structure–activity relationship (QSAR) as rationale basis for the VAChT ligand optimization.

In the present work, the first quantitative model for the VAChT binding affinity of vesamicol derivatives has been derived. To this end, three-dimensional (3D) comparative molecular field analysis (CoMFA[37,38]) studies have been performed for a set of 37 vesamicol derivatives taken from literature,[13,39–44] covering three different structural types according to substitutions at the three different rings of vesamicol

* To whom correspondence should be addressed. Tel.: +49-341-235-1262. Fax: +49-341-235-1785. E-mail: gerrit.schuurmann@ufz.de.

[†] UFZ Helmholtz Centre for Environmental Research.

[‡] Institute of Interdisciplinary Isotope Research.

[§] Technical University Bergakademie Freiberg.

[a] Abbreviations: VAChT, vesicular acetylcholine transporter; PET, positron emission tomography; SPECT, single photon emission computed tomography; QSAR, quantitative structure–activity relationship; 4-PHP, 4-phenylpiperidine derivatives of vesamicol; spiro, spirovesamicol derivatives; tropan, tropanvesamicol derivatives; CoMFA, comparative molecular field analysis; 3D, three-dimensional; PLS, partial least-squares; LOO, leave-one-out cross-validation; LO50, leave out 50%; q^2, predictive squared correlation coefficient; s_p, predictive standard error (without consideration of degrees of freedom).

10.1021/jm700961r CCC: $40.75
Published on Web 03/07/2008

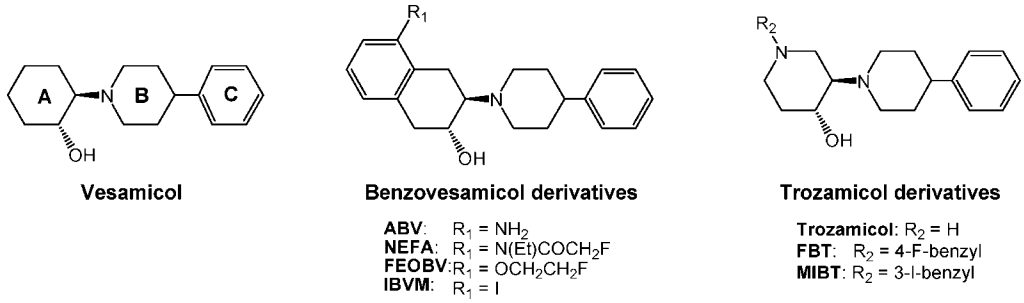

Figure 1. Selected known ligands for the vesicular acetylcholine transporter (VAChT).

Table 1. Calibration and Prediction Statistics of CoMFA Models for Conformer Set 1 (Lowest-Energy Conformations)[a]

training set	No. training cmpds	CoMFA steric fraction[b]	r^2	s	q^2 (LOO)[c]	s_p (LOO)[c]	No. predicted cmpds (EXT)[d]	q^2 (EXT)[d]	s_p (EXT)[d]
all	37	0.47	0.80	0.63	0.66	0.82	[e]	[e]	[e]
nonspiro	23	0.49	0.88	0.51	0.64	0.88	23	0.47	1.05
nontropan	29	0.49	0.80	0.61	0.64	0.83	8	0.43	1.25
group I	19	0.51	0.84	0.62	0.57	1.01	18	0.74	0.65
group II	18	0.45	0.90	0.43	0.63	0.86	19	0.59	0.94
group III	19	0.49	0.84	0.64	0.47	1.15	18	0.74	0.64
group IV	18	0.46	0.89	0.45	0.65	0.82	19	0.65	0.88

[a] All CoMFA[37,38] models employ two PLS[45] components (latent variables) and are characterized by the following statistical parameters: r^2 = squared correlation coefficient, s = standard error (without consideration of degrees of freedom), q^2 = predictive squared correlation coefficient (eq 1), s_p = standard error of prediction (eq 2, without consideration of degrees of freedom). [b] Relative contribution of steric CoMFA field (adds up to 1 with the electrostatic CoMFA field contribution). [c] Leave-one-out cross-validation[46] as applied to partial least-squares (PLS) regression. [d] Simulated external validation[50] through predictive application to complementary subsets: spiro compounds predicted by nonspiro model; tropan compounds predicted by nontropan model; group I predicted by model calibrated with group II compounds and vice versa; group III compounds predicted by model calibrated with group IV compounds and vice versa. [e] Not applicable.

(see Figure 1 and Table 3). The results unravel structural implications for high VAChT binding affinities and thus provide guidance for future synthetic work in this area.

Data Set of Compounds and Binding Affinities

Set of Compounds and Experimental Data. Vesamicol contains three substructural units (Figure 1): the cyclohexyl ring A, the piperidyl moiety B, and the phenyl ring C. For the derivation of our quantitative model, vesamicol (**1**) and 36 derivatives (**2**−**37**) with modifications in the fragments A, B, and C were taken into account as shown in Figure 2.

The first class of 4-phenylpiperidine derivatives (4-PHP) contains compounds that are characterized by modifications in the cyclohexyl ring A, while retaining the 4-phenylpiperidine moiety (**1**−**15** in Figure 2). Besides vesamicol (**1**), the well-known ligands, 4-*tert*-butylvesamicol (**5**), *trans*-decahydronaphthalenevesamicol (**6**), and benzovesamicol (**7**), belong to this subset. The second class (spiro class) consists of 14 spirovesamicol derivatives (**16**–**29**) that are modified in ring B and ring C and, in some cases, also in the cyclohexyl ring A. These compounds form a class of conformationally restricted vesamicol analogs, in which the rotation of the phenyl moiety relative to the piperidyl moiety is hindered, and where the two rings take up an orthogonal orientation. Tropanvesamicol derivatives (tropan class, **30**–**37**) form the third class, and are conformationally restricted at ring B by replacing the 4-phenylpiperidyl fragment of vesamicol by the 3β-phenyltropanyl fragment. Moreover, these compounds contain ring A modifications.

For all 37 compounds, K_i values as quantitative measures of the binding affinity were taken from literature[21,39–44] (see Table 3). These experimental data were measured through competition against the binding of (±)-[^{3}H]vesamicol to electric organ synaptic vesicles according to the method of Rogers et al.[21] For the CoMFA modeling, log K_i [nM] values were employed. The data span a range of 5.5 orders of magnitude, with minimum and maximum log K_i values of −2.05 (0.009 nM, **6** in Figure 2) and 3.53 (3400 nM, **33**), corresponding to free energies of binding at 25 °C of −63.0 and –31.2 kJ/mol, respectively.

Results and Discussion

CoMFA Model Calibration and LOO Cross-Validation. In vesamicol and its derivatives, the OH group of the cyclohexyl ring A (see Figure 1) can be in the axial or equatorial position. Accordingly, geometry optimization was performed for both the axial and equatorial conformer of all compounds, and the following four sets of conformers were generated for CoMFA model building: set 1, consisting of the lowest-energy conformations (with OH in axial position in most but not all cases), set 2, where all compounds have OH in axial position, set 3, where OH is in equatorial position throughout, and set 4, consisting of the higher-energy conformations with respect to the OH position (with OH in equatorial position in most but not all cases). For the 37 compounds under investigation, the calculated difference in energy between the axial and the equatorial conformers is quite low with 1.5 kJ/mol on the average and with individual values ranging from 0.2 to 5.6 kJ/mol, respectively.

Employing partial least-squares (PLS) regression[45] with leave-one-out (LOO) cross-validation[46] to minimize the number of PLS components (latent variables) while maximizing q^2 (predictive squared correlation coefficient, see eq 1), two latent variables turned out to yield the best PLS model for conformer sets 1 and 2, while one latent variable was already sufficient for sets 3 and 4, respectively. Conformer set 1 (lowest-energy conformers) yields the overall best CoMFA statistics, which are summarized in Table 1. The associated LOO statistics (q^2 (LOO) = 0.66, s_p = 0.82 log units; see Table 1) suggest a reasonable prediction power suitable to support VAChT ligand design in experimental work and are also still comparable to the calibration statistics (r^2 = 0.80, and s = 0.63 log units). The data distribution of calibrated and LOO-predicted versus experimental log K_i data is shown in Figure 3.

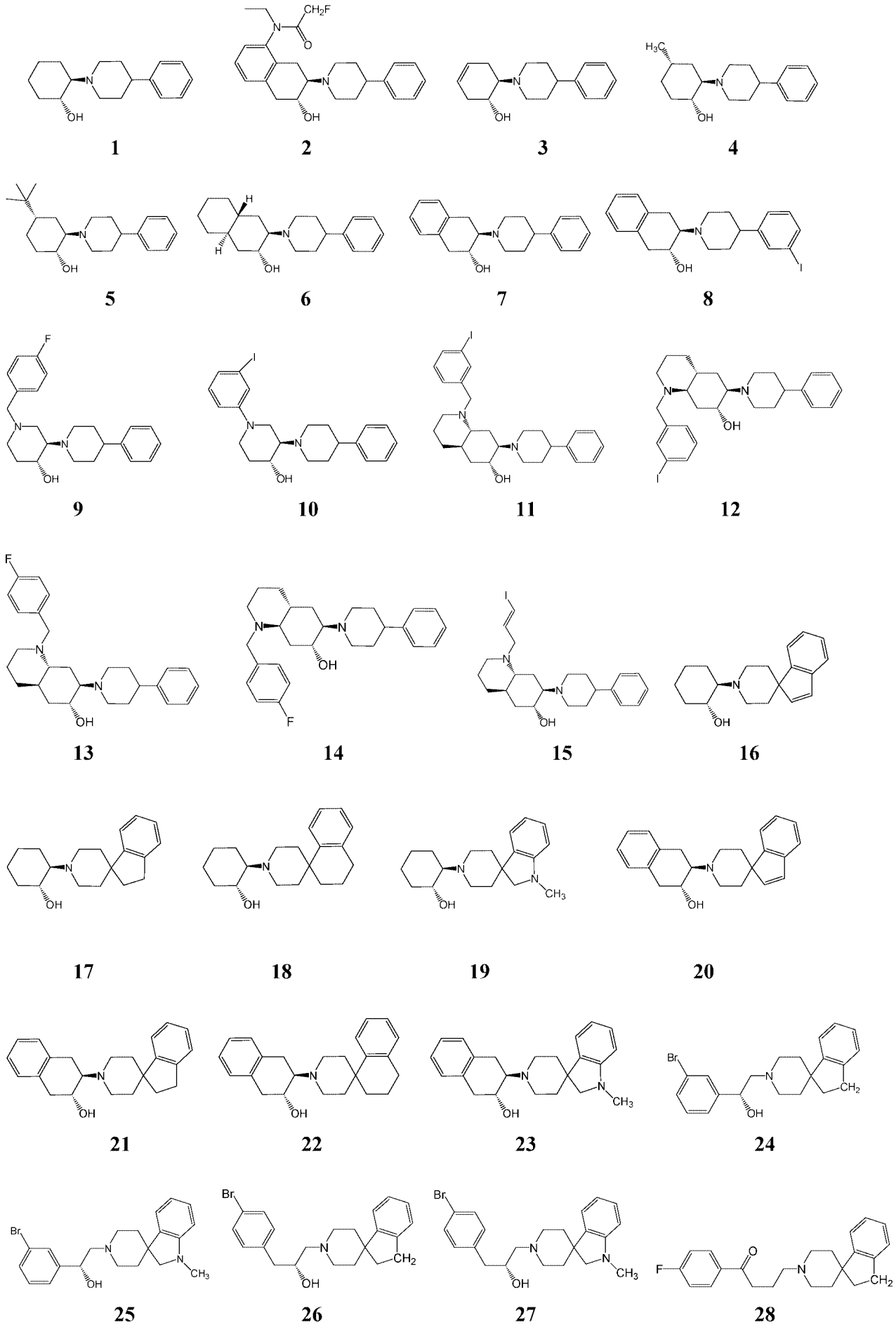

Figure 2 (continued on next page)

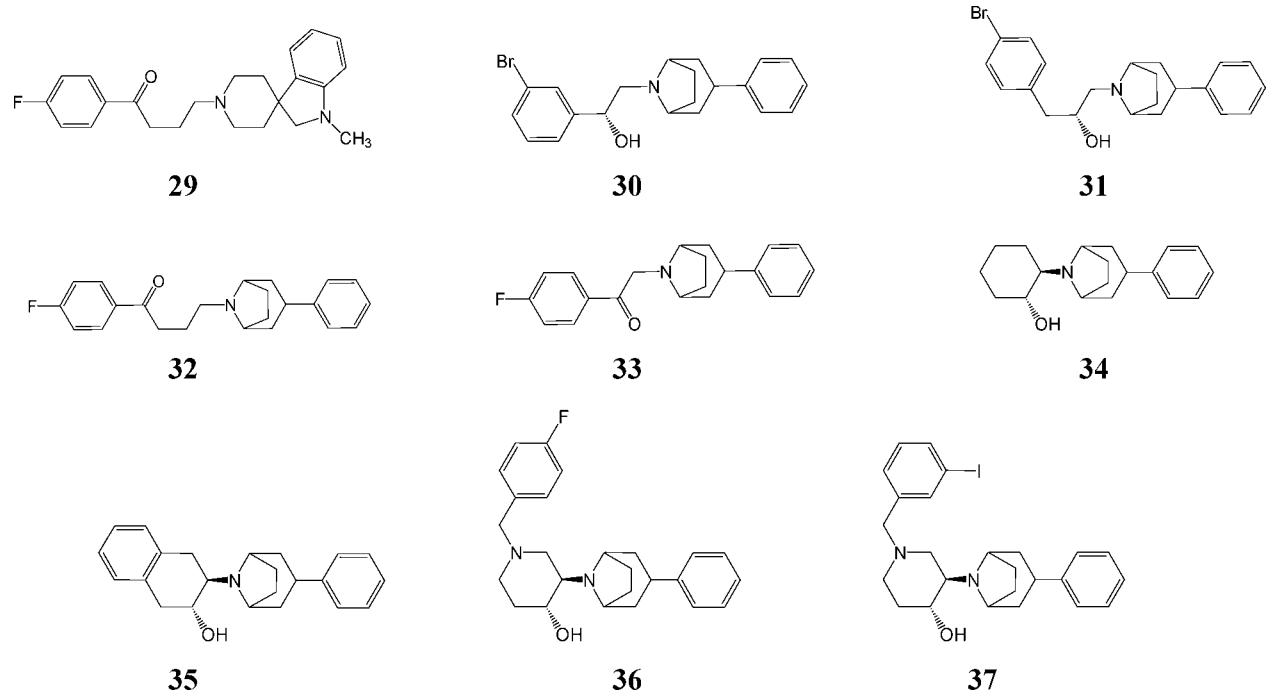

Figure 2. Molecular structures of vesamicol (**1**) and 36 vesamicol derivatives for which experimental binding affinities (K_i values) were available from literature.[21,39–44]

Table 2. Calibration and Prediction Statistics of CoMFA Models for Conformer Sets 2 (A-Ring OH Only in Axial Position), 3 (A-Ring OH Only in Equatorial Position), and 4 (Higher-Energy Conformers with Respect to OH Position)

conformer set	No. of latent variables	CoMFA steric fraction[a]	r^2	s	q^2 (LOO)[b]	s_p (LOO)[b]
2	2	0.51	0.80	0.64	0.62	0.87
3	1	0.46	0.72	0.74	0.62	0.86
4	1	0.49	0.73	0.72	0.63	0.85

[a] Relative contribution of steric CoMFA field (adds up to 1 with the electrostatic CoMFA field contribution). [b] Leave-one-out cross-validation[46] as applied to partial least-squares (PLS) regression.

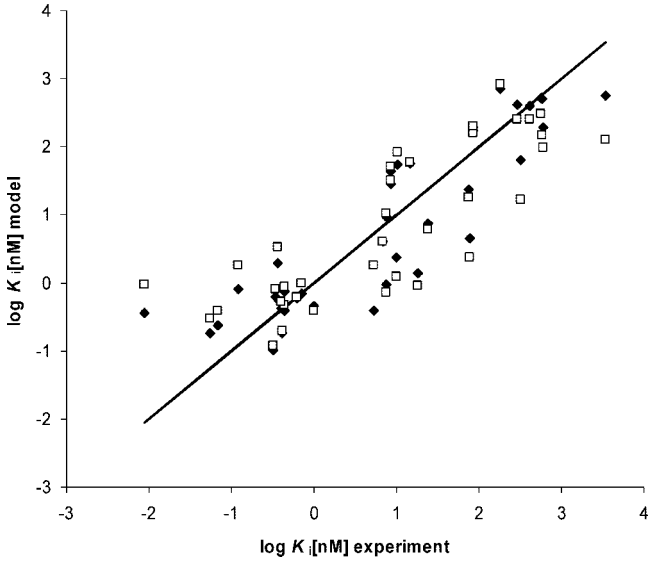

Figure 3. CoMFA predicted vs experimental log K_i values (binding affinities) of 37 vesamicol compounds as VAChT ligands (conformer set 1, model ALL), including the regression line $y = x$. □ = LOO prediction ($q^2 = 0.66$), ♦ = calibration ($r^2 = 0.80$).

As expected, omission of the spiro compounds yields a model that is less useful for predicting log K_i of spiro derivatives (q^2 (EXT) = 0.47). A corresponding situation holds for the nontropan model (Table 1, row 3).

The findings indicate that across the presently analyzed derivatives of vesamicol, the variation in the steric and electrostatic fields appears to be somewhat similar, which merits further attention in future 3D QSAR studies of vesamicol derivatives as potential VAChT ligands.

Axial versus Equatorial OH Position. To address the influence of the conformer position of the A-ring OH group, CoMFA models have also been developed for conformer sets 2 (axial position only), 3 (equatorial position only), and 4 (higher-energy conformers with respect to OH position). The respective CoMFA statistics are summarized in Table 2. Sets 2–4 yield very similar LOO q^2 values (0.62 – 0.63) and predictive standard errors s_p (0.85 – 0.87), both of which are somewhat inferior to the ones achieved with the lowest-energy conformations ($q^2 = 0.66$, $s_p = 0.82$, see Table 1). Within the presently used model framework (SYBYL Tripos force field, Gasteiger−Hückel net atomic charges[47]), the results suggest that, in most but not all cases, the axial OH position is preferred for the VAChT binding of vesamicol derivatives and that the conformer preferred for VAChT binding is the one with lowest energy.

Simulated External Validation. Because no additional compounds outside the present training set were available, the external prediction power of the CoMFA models could not be tested directly. At the same time, LOO cross-validation alone is not a reliable indicator of the prediction capability of QSAR models for two well-known reasons: LOO tends to reflect more the model robustness than its prediction power, and LOO yields increasingly optimistic results with increasing data set size (simply because removing one compound from a large data set will generally result in little if any variation of its structural domain).[48] Moreover, LOO cross-validation does not show the correct asymptotic trend with increasing number of observations.[49]

Table 3. Experimental and CoMFA Predicted log K_i Values (binding affinities) of 37 Vesamicol Compounds as VAChT Ligands[a]

		calibration			LOO prediction (LOO cross-validation)			simulated external prediction (LO50)	
cmpd No.	experimental log K_i [nM]	all	groups I + II	groups III + IV	all	groups I + II	groups III + IV	groups I + II	groups III + IV
1	0.88	−0.03	−0.01[b]	−0.01[d]	−0.14	−0.27[b]	−0.23[d]	−0.04[c]	0.14[e]
2	−0.49	−0.99	−0.93[b]	−0.94[e]	−0.92	−0.85[b]	−0.86[e]	−1.00[c]	−0.78[d]
3	−0.47	−0.20	−0.45[c]	−0.19[e]	−0.09	−0.23[c]	0.07[e]	0.01[b]	−0.03[d]
4	−0.20	−0.23	−0.23[c]	−0.27[d]	−0.20	−0.14[c]	−0.23[d]	−0.22[b]	0.00[e]
5	−1.17	−0.62	−0.75[b]	−0.83[d]	−0.40	−0.32[b]	−0.41[d]	−0.46[c]	−0.24[e]
6	−2.05	−0.44	−0.67[b]	−0.68[d]	−0.02	0.15[b]	0.13[d]	−0.18[c]	−0.03[e]
7	−1.26	−0.74	−1.10[c]	−0.70[e]	−0.53	−0.64[c]	−0.20[e]	−0.43[b]	−0.67[d]
8	−0.38	−0.74	−0.45[b]	−0.74[d]	−0.70	−0.21[b]	−0.55[d]	−1.09[c]	−0.66[e]
9	−0.36	−0.13	−0.10[c]	−0.22[e]	0.06	0.33[c]	0.13[e]	−0.14[b]	0.25[d]
10	−0.15	−0.16	−0.07[b]	−0.16[e]	−0.01	0.20[b]	0.13[e]	−0.24[c]	−0.03[d]
11	−0.36	−0.40	−0.56[b]	−0.35[e]	−0.32	−0.40[b]	−0.08[e]	−0.21[c]	−0.18[d]
12	0.72	0.41	0.76[b]	0.45[e]	0.26	0.45[b]	0.19[e]	0.11[c]	0.46[d]
13	0.00	−0.34	−0.19[c]	−0.14[d]	−0.40	−0.23[c]	−0.25[d]	−0.47[b]	−0.26[e]
14	1.00	0.38	0.75[b]	0.48[d]	0.09	0.20[b]	−0.23[d]	0.06[c]	0.38[e]
15	−0.40	−0.37	−0.28[c]	−0.30[d]	−0.27	0.01[c]	−0.08[d]	−0.46[b]	−0.20[e]
16	0.84	0.60	0.63[c]	0.42[d]	0.60	0.61[c]	0.38[d]	0.59[b]	0.88[e]
17	0.88	0.98	1.16[c]	1.00[e]	1.02	1.24[c]	1.09[e]	0.79[b]	1.10[d]
18	1.38	0.88	0.69[b]	0.94[e]	0.79	0.44[b]	0.75[e]	1.06[c]	0.92[d]
19	1.87	1.37	1.45[c]	1.34[d]	1.25	1.16[c]	1.02[d]	1.24[b]	1.49[e]
20	−0.92	−0.09	−0.37[c]	−0.25[d]	0.26	0.33[c]	0.62[d]	0.15[b]	0.08[e]
21	−0.44	0.29	0.32[b]	0.20[e]	0.53	1.02[b]	0.70[e]	0.18[c]	0.42[d]
22	1.26	0.15	0.04[c]	0.21[d]	−0.04	−0.40[c]	−0.19[d]	0.19[b]	0.11[e]
23	1.89	0.65	0.77[b]	0.69[e]	0.38	0.22[b]	0.05[e]	0.42[c]	0.61[d]
24	2.78	2.28	2.54[c]	2.60[d]	1.98	1.91[c]	1.90[d]	1.86[b]	1.93[e]
25	2.26	2.85	2.57[b]	2.60[e]	2.92	2.64[b]	2.60[e]	2.92[c]	3.01[d]
26	1.93	2.23	2.06[c]	1.89[e]	2.21	1.71[c]	1.58[e]	2.22[b]	2.64[d]
27	2.62	2.61	2.66[b]	2.85[d]	2.40	2.26[b]	2.51[d]	2.34[c]	2.38[e]
28	1.93	2.28	1.90[b]	2.14[d]	2.31	1.73[b]	2.05[d]	2.62[c]	2.32[e]
29	2.76	2.72	2.97[c]	2.87[e]	2.48	2.19[c]	2.29[e]	2.39[b]	2.44[d]
30	2.47	2.62	2.47[c]	2.36[e]	2.41	1.92[c]	1.79[e]	2.47[b]	2.85[d]
31	1.01	1.74	1.33[c]	1.58[d]	1.92	1.58[c]	2.06[d]	1.98[b]	1.76[e]
32	2.77	2.70	3.20[b]	2.69[e]	2.17	2.57[b]	1.57[e]	1.71[c]	2.62[d]
33	3.53	2.76	3.19[b]	3.32[d]	2.10	2.13[b]	1.92[d]	1.93[c]	2.17[e]
34	0.93	1.64	1.43[b]	1.83[d]	1.71	1.56[b]	2.06[d]	1.68[c]	1.46[e]
35	0.93	1.46	1.46[c]	1.28[e]	1.51	1.62[c]	1.33[e]	1.27[b]	1.69[d]
36	2.51	1.80	2.24[c]	2.49[d]	1.23	0.91[c]	1.24[d]	1.23[b]	1.23[e]
37	1.16	1.75	1.22[b]	1.23[e]	1.78	0.92[b]	0.90[e]	2.17[c]	2.43[d]

[a] Molecular structures of the compounds are shown in Figure 2. Experimental log K_i [nM] values[21,39–44] refer to measuring competition against the binding of (±)-[^{3}H]vesamicol to electric organ synaptic vesicles according to the method of Rogers et al.[21] LOO = leave-one-out.[46] Simulated external validation:[50] LO50 = leave 50% out; the CoMFA[37,38] model calibrated with group I (19 compounds, see text and table footnote b) was used to predict log K_i of group II compounds (18 compounds, see table footnote c) and vice versa, and correspondingly, the CoMFA model calibrated with group III (19 compounds, see table footnote d) was used to predict log K_i of group IV compounds (18 compounds, see table footnote e) and vice versa. [b] Group I. [c] Group II. [d] Group III. [e] Group IV.

Accordingly, we decided to apply a more stringent test of the prediction capability by increasing the portion of left-out compounds to 50% following a selection procedure introduced earlier.[50] After ordering the compounds according to decreasing log K_i (increasing binding affinity), the odd- and even-numbered compounds were allocated to two different subsets of 19 and 18 compounds, respectively. Application of this approach to the total compound set resulted in groups I and II, while its stratified application for each of the three different compound classes (4-PHP, spiro, tropan) led to groups III and IV, respectively. Group I contains 9 4-PHP, 6 spiro, and 4 tropan compounds, and group II contains 6 PHP, 8 spiro, and 4 tropan compounds: group I: **1**, **2**, **5**, **6**, **8**, **10**, **11**, **12**, **14**, **18**, **21**, **23**, **25**, **27**, **28**, **32**, **33**, **34**, **37**; group II: **3**, **4**, **7**, **9**, **13**, **15**, **16**, **17**, **19**, **20**, **22**, **24**, **26**, **29**, **30**, **31**, **35**, **36**.

Groups III and IV both contain 7 spiro and 4 tropan derivatives and differ only in the number of 4-PHP derivatives (8 in group III and 7 in group IV): group III: **1**, **4**, **5**, **6**, **8**, **13**, **14**, **15**, **16**, **19**, **20**, **22**, **24**, **27**, **28**, **31**, **33**, **34**, **36**; group IV: **2**, **3**, **7**, **9**, **10**, **11**, **12**, **17**, **18**, **21**, **23**, **25**, **26**, **29**, **30**, **32**, **35**, **37**.

Due to the activity-related ordering, the subsets of odd- and even-numbered compounds cover a similar range of (measured) target property values, as is reflected by the group-specific mean values for log K_i (0.84 for I and III and 0.87 for II and IV, respectively). Therefore, potential problems in interpreting q^2 in case of substantial differences between the training set mean and the validation set mean can be avoided.[50]

The results are summarized in the last two columns of Tables 1 (statistics) and 3 (predicted values) for conformer set 1 (lowest-energy conformations). For conformer sets 2–4, the statistics are generally similar and typically somewhat inferior (details not shown). The CoMFA model trained only with the 19 group I compounds ($r^2 = 0.84$, $s = 0.62$) yields $q^2 = 0.74$ and $s_p = 0.65$ for the 18 group II compounds, demonstrating a significant prediction capability over (almost) the whole range of the target property as well as across all three compound classes. Slightly different statistics are obtained for the group II-calibrated model ($r^2 = 0.90$) used to predict group I compounds ($q^2 = 0.59$), for the group III-calibrated model ($r^2 = 0.84$) used to predict group IV compounds ($q^2 = 0.74$), and for the group IV-calibrated model ($r^2 = 0.89$) used to predict group III compounds ($q^2 = 0.65$).

Note further that when considering all 37 predicted values of the second−last columns of Table 3 (predictions for all 19 group I compounds provided by the group-II model and predictions for all 18 group II compounds provided by the

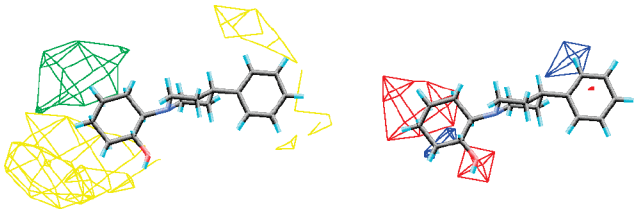

Figure 4. Contour maps of critical regions of the CoMFA steric (left) and electrostatic (right) fields with vesamicol (**1**) as reference compound. Left: yellow contours indicate regions where steric repulsion decreases binding affinity, while the green area represents a region with favorable steric interaction. Right: blue contours indicate an increase in binding affinity with increasing positive charge of the ligand, and in regions with red contours, increasing negative charge is increasingly favorable for binding.

group-I model), $q^2 = 0.62$ and $s_p = 0.83$, which is close to the LOO result for the all-compound CoMFA model ($q^2 = 0.65$, $s_p = 0.80$). The corresponding results for the combined group III and group IV predictions (taking together all data from the last column of Table 3) are even better with $q^2 = 0.69$ and $s_p = 0.76$. These findings demonstrate that the 37-compound CoMFA model is robust and that it has indeed a substantial prediction capability.

Interestingly, the LOO cross-validation results achieved for groups I and III are less successful, as indicated by relatively low q^2 values of 0.57 and 0.47, respectively. Note that these only moderate LOO results contrast sharply with the much better LO50 results obtained with these two groups (when predicting all compounds of group II and group IV, respectively). Detailed investigation reveals that both groups I and III contain *trans*-decahydronaphthalenevesamicol (**6**) as outlier. This accounts also for the fact that LO50-based predictions for these two groups yield lower q^2 values (around 0.6) than corresponding predictions for two other groups (0.74). In any case, future 3D QSAR investigations of respective classes of vesamicol-type ligands should pay attention to the LOO results as compared to LO50 results.

Contour Plots Highlighting Critical Steric and Electrostatic Regions. Contour plots of site-specific interaction energies evaluated at the lattice points between the probe atom and the molecule of interest (here: vesamicol-type ligands for VAChT) allow one to visualize regions in 3D molecular space where an increase in the relevant CoMFA field (steric or electrostatic) leads to an increase or decrease of the target property (in our case: binding affinity in terms of log K_i). Respectively, critical regions thus provide information about how a change in molecular structure is likely to affect its binding affinity and about the steric and electrostatic characteristics of the VAChT binding site.

In Figure 4, contour plots of steric (left) and electrostatic (right) field regions increasing and decreasing the binding affinity are visualized with vesamicol as reference compound. On the left, favorable steric bulk is shown in green, while the yellow contours identify regions where increasing steric bulk corresponds to increasing van der Waals repulsion, and thus decreases the binding affinity to VAChT. On the right, blue contours are located at molecular sites where an increase in positive charge increases the binding affinity (decreases log K_i), and the red contours represent regions where the binding affinity is increased (log K_i decreased) with increasing negative charge.

According to this analysis, sterically unfavorable regions are found around the cyclohexyl ring A near the hydroxyl group and close to phenyl ring C (compare also Figure 1). By contrast, an increase of steric bulk in the region of cyclohexyl ring A diagonally opposite to the hydroxyl group favors binding to VAChT. With regard to Coulomb interactions, positive charge around ring A on the side of the OH group and close to ring C supports binding, and a respective favorable interaction takes place increasingly with increasing negative charge at the opposite side of ring A and inside the OH group region. Note further that sterically favorable regions (green) overlap with regions favorable through negative charge (red), and a similar overlap in 3D molecular space is observed between sterically unfavorable regions (yellow) and regions favorable for positive charge (blue), except for the OH-group region.

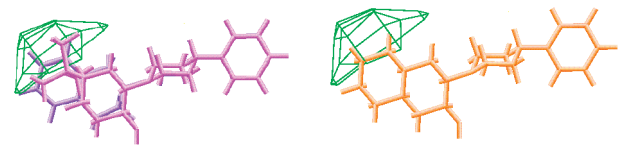

Figure 5. Favorable (green) region of the CoMFA steric field in relation to *tert*-butylvesamicol (**5**) and benzovesamicol (**7**, left) as well as to *trans*-decahydronaphthalenevesamicol (**6**, right), respectively. In contrast to **5** and **7**, the molecular skeleton of **6** does not enter the sterically favorable region.

Poor Prediction of Strongest Ligand. Despite overall good statistics for both calibration and prediction, a current drawback is the fact that *trans*-decahydronaphthalenevesamicol (**6**) as ligand with greatest binding affinity (log K_i [nM] = −2.05) is among the greatest outliers of the CoMFA model calibrated with all compounds. Here, the experimental binding affinity is underpredicted by 1.4–2.2 log units (see Table 3). By contrast, *tert*-butylvesamicol (**5**, log K_i [nM] = −1.17) and benzovesamicol (**7**, log K_i [nM] = −1.26), as two additional high-affinity ligands of the 4-PHP type, fit substantially better (though still not perfectly) to the presently derived CoMFA models (underestimation of binding affinity by 0.3–1.0 log units, see Table 2).

As can be seen from the left part of Figure 5, the *tert*-butyl group of **5** and the aromatic ring of **7** overlap with the region sterically favorable for high binding affinity (green contours). Compound **6**, however, has no extended molecular part in this sterically favorable area (right part of Figure 5). Keeping in mind that the molecular characteristics of **6** are not covered well by the present CoMFA model, this geometric analysis suggests that alkyl substitution at the back side of the decahydronaphthalene moiety (orientation guided through Figure 5) is likely to still increase its binding affinity.

Reduced Binding Affinity of Spirovesamicols. In general, experimental log K_i values of conformationally restricted spirovesamicols are higher than the average of all compounds (see Table 3), indicating a generally lower binding affinity toward VAChT. From the viewpoint of the presently derived CoMFA model, this can be traced back to the fact that the additional junction between the phenyl and the piperidyl moieties is located close to the region identified as sterically unfavorable (yellow contour) for high binding affinities.

This effect is illustrated in Figure 6 comparing benzovesamicol (**7**, log $K_i = -1.26$) with its spiro analogs **21** (log $K_i = -0.44$) and **22** (log $K_i = 1.26$). Substitution of the spiro moiety extends the molecular structure toward a sterically unfavorable region (yellow contours) that cannot be avoided due to the conformational restriction associated with this structural type. Accordingly, increasing nonpolar substitution at the spiro compound is likely to increasingly reduce the binding affinity toward VAChT.

Tropan Effect on Binding Affinity. Another type of conformational restriction, whose influence on the binding affinity

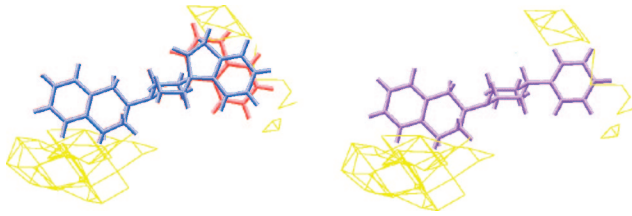

Figure 6. Spiro effect illustrated by ligands **21** and **22** (blue and red, left) and their nonspiro analog benzovesamicol **7** (purple, right) in relation to unfavorable (yellow) steric CoMFA contour lines that indicate repulsive interaction with the VAChT binding site. Substitution at the spiro moiety extends the molecular structure towards the repulsive steric region.

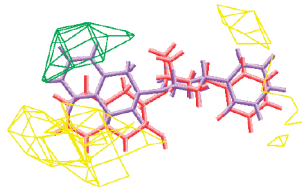

Figure 7. Tropan effect illustrated by comparing benzovesamicol (**7**, purple) and its tropan analog **35** (red) with the critical regions of the CoMFA steric field (green = favorable, yellow = unfavorable). The ethylene bridge of the tropan analog imposes a conformation that reduces its molecular extension in the sterically favorable region.

is reflected in the CoMFA model, is caused by the introduction of an ethylene bridge in the piperidyl ring B. Due to this structural modification, the interconversion of piperidine conformers is prevented. In general, the resulting 3β-phenyltropanyl derivatives of vesamicol are characterized by reduced binding affinities toward VAChT as compared to nontropan analogs.

An example is given by the high-affinity compound benzovesamicol (**7**, log $K_i = -1.26$) as compared to its tropan analog **35** (log $K_i = 0.93$; see Table 2), the latter of which exhibits a much lower binding affinity toward VAChT. The CoMFA rationale for this tropan effect is illustrated in Figure 7. While the benzocyclohexyl moiety of **7** is located in the region of favorable steric interaction with the VAChT binding site (green contour lines), the corresponding moiety of tropan analog **35** is pushed away from this favorable region due to the conformation imposed by the ethylene bridge. In addition, an electrostatic effect contributes to the reduced binding affinity of tropan derivatives. In the nontropan analogs, the negatively charged OH group of the cyclohexyl ring is closer to the VAChT site, where increasing negative charge increasingly favors binding of the ligand.

A further example of the tropan effect is given by comparing **9** and **36** as a further pair of structural counterparts. Here, the binding affinities differ by almost 3 orders of magnitude (log K_i values of -0.36 and 2.51, respectively; see Table 2).

Regioisomers. Configurational features are another well-known factor influencing the binding affinity. In the case of the decahydrochinoline derivatives **11**–**14**, two pairs of regioisomeres can be considered. Both **13** (log K_i [nM] = 0.00) and **14** (log K_i [nM] = 1.00) have a fluorobenzyl group bound to ring nitrogen, but they differ in their spatial position with respect to the bicyclic ring system (see structures in Figure 2).

The CoMFA results presented in Figure 8 provide an explanation for the significant differences in binding affinity of these two ligands. In **13**, which is more potent as ligand by a factor of 10, the fluorobenzyl group is close to the favorable (green) region, whereas in **14** it is more directed toward the unfavorable (yellow) region. The differences in binding affinity between the regioisomeres **11** and **12** can be elucidated in a similar way.

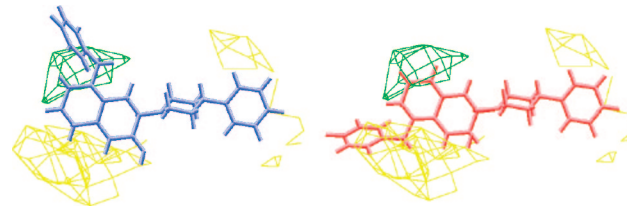

Figure 8. Two regioisomers of decahydrochinolines **13** (blue, left) and **14** (red, right) in relation to critical regions of the CoMFA steric field. The 4-fluorobenzyl moiety of **13** is close to the favorable (green) steric region, while in **14** it is oriented towards the unfavorable (yellow) region.

N-CH_3 Effect in Spiro Compounds. In some spiro compounds, one cyclopentyl CH_2 unit is replaced by N-CH_3 (**19**, **23**, **25**, **27**, and **29**; see Figure 2). This structural modification is accompanied by increased log K_i values corresponding to decreased binding affinities (see Table 3). Inspection of the CoMFA electrostatic field reveals that the negatively charged N-CH_3 unit is close to a region where positive ligand charge would support binding to VAChT.

Conclusions

The CoMFA models developed relate, for the first time, structural features of vesamicol-type ligands to their binding affinity toward VAChT in a quantitative manner. As such, they provide a new rationale for designing vesamicol derivatives as highly potent VAChT ligands. Due to the 3D QSAR approach, detailed insight into structural implications for high binding affinity has become available, and correspondingly low affinities observed for various ligand candidates can now be traced back to critical features of their molecular structures. While the present study focused on binding affinity, a second prerequisite for vesamicol derivatives as successful radiotracers to image cholinergic dysfunctions is an additional optimization of their selectivity for VAChT. Recent CoMFA and CoMSIA (comparative molecular similarity indices analysis) work on ligands for imaging alterations of dopaminergic signal pathways[51] suggests that future 3D QSAR studies may provide a rationale basis also for improving the VAChT selectivity of vesamicol-type ligands, which would augment our presently derived CoMFA model for the development of clinically relevant radiotracers of the vesamicol type.

Experimental Section

Generation of 3D Molecular Structures. Starting structures were generated using CORINA.[52] Subsequent geometry optimization was performed employing the TRIPOS force field of SYBYL[47] and its implementation of the BFGS routine, considering both the equatorial and the axial position of the OH group in ring A. Gasteiger−Hückel partial charges were added to provide electrostatic fields. Subsequently, four different sets of conformers were generated: The first and major set is given by the conformers yielding the lowest energy (where OH is axial in most but not all cases), set 2 consists of all conformers with OH in the axial position, set 3 consists of all conformers with OH in the equatorial position, and set 4 consists of all compounds in the higher-energy conformation with respect to the OH group (where OH is in equatorial position in most but not all cases).

CoMFA Preparation. For the 3D alignment of the geometry-optimized compounds, ring B (the 4-piperidyl moiety, see Figure 1) of vesamicol was used as reference structure, employing the root-mean-square-based MATCH feature of SYBYL.

Steric and electrostatic CoMFA fields were calculated using a sp^3 carbon with a charge of +1 as probe atom, employing a grid size of 2.0 Å and a total lattice size such that the Cartesian coordinates of all compounds were exceeded by at least 4 Å in all directions. The van der Waals 6–12 potential TRIPOS parameters (atomic radii) were used for the steric interaction energies, and the electrostatic fields were calculated based on the Gasteiger−Hückel net atomic charges of the molecules. A cutoff value of 50 kcal/mol was used for both the steric and the electrostatic interaction energies. Electrostatic interaction at grid points with steric cutoff values were set to the mean of all nonexcluded electrostatic values. The type of transition between the cutoff plateaus was set to "smooth", that is, there was an interpolation from 6 kcal/mol below the cutoff to the plateau.

PLS-Based CoMFA Model Derivation. Model derivation employing partial least-squares (PLS) regression was guided by leave-one-out (LOO) cross-validation to determine the optimal number of components to be used for the final noncross-validated PLS model. Only the subset of CoMFA field sample points with a standard deviation ≥0.5 kcal/mol (σ_{min} value for column filtering) was taken to perform PLS regression, which turned out as best value according to tests performed on σ_{min} values between 0.1 and 5.0 kcal/mol. Corresponding tests performed on scaling methods showed that an overall best performance of the CoMFA standard scaling, applying autoscaling to the steric and electrostatic fields separately.

Model Evaluation. The prediction quality was evaluated using the predictive squared correlation coefficient, q^2,

$$q^2 = 1 - \frac{\sum_i \left(y_i^{pred} - y_i^{obs}\right)^2}{\sum_i \left(y_i^{obs} - y^{mean}\right)^2} \quad (1)$$

where y_i^{pred}, y_i^{obs}, and y^{mean} are the predicted (not fitted), actual, and mean values of the target property (in our case: log K_i), and the associated standard error of prediction, s_p,

$$s_p = \left[\frac{1}{N}\sum_i \left(y_i^{pred} - y_i^{obs}\right)^2\right]^{\frac{1}{2}} \quad (2)$$

where N denotes the number of compounds (without consideration of the degrees of freedom). These statistical measures were used for both LOO and when predicting 50% of the compounds that were left out for model calibration, LO50, as outlined in the next section. Note that the nominator in eq 1 represents the predictive sum of squares (PRESS), while the denominator is often referred to as sum of squares (SS).

The calibration quality of the final (noncross-validated) models was assessed through the squared correlation coefficient, r^2 (where y_i^{pred} in eq 1 would be replaced by y_i^{fit}, the fitted value for the target property), and its standard error s (correspondingly, replacing y_i^{pred} in eq 2 by y_i^{fit}).

Simulated External Validation. Due to the lack of additional vesamicol derivatives, the prediction power of the presently derived CoMFA models was further evaluated using a procedure introduced earlier.[50] First, the compound set was divided into two subsets, each of which contains (almost) 50% of the compounds (LO50), as outlined below. Second, these two subsets were used for both calibration and prediction such that the model calibrated by one subset (e.g., group I) was used to predict the activities of all compounds of the other subset (e.g., group II).

For the subset generation, the following two variants of our approach based on the activity ordering of the compounds were applied: (1) The compounds were ordered according to decreasing log K_i (increasing binding affinity) and then subdivided into the group of odd- and even-numbered subsets (groups I and II, respectively); (2) the same procedure was applied within each of the three structurally different classes (4-PHP, spiro, and tropan), and then the odd-numbered compounds of each class were put into one subset (group III) and the even-numbered compounds into the other subset (group IV). In this way, the total set of 37 compounds was divided, in two different ways, into 19 odd-numbered and 18 even-numbered compounds.

Acknowledgment. Financial support was provided by the Deutsche Forschungsgemeinschaft (DFG), Contract No. WE2927/1-1.

References

(1) Davies, P.; Maloney, A. J. Selective loss of central cholinergic neurons in Alzheimer's disease. *Lancet* **1976**, *2*, 1403.
(2) Coyle, J. T.; Price, D. L.; DeLong, M. R. Alzheimer's disease: A disorder of cortical cholinergic innervation. *Science* **1983**, *219*, 1184–90.
(3) Lleo, A.; Greenberg, S. M.; Growdon, J. H. Current pharmacotherapy for Alzheimer's disease. *Annu. Rev. Med.* **2006**, *57*, 513–33.
(4) Scarpini, E.; Scheltens, P.; Feldman, H. Treatment of Alzheimer's disease: Current status and new perspectives. *Lancet Neurol.* **2003**, *2*, 539–547.
(5) Eiden, L. E.; Schäfer, M. K.; Weihe, E.; Schütz, B. The vesicular amine transporter family (SLC18): Amine/proton antiporters required for vesicular accumulation and regulated exocytotic secretion of monoamines and acetylcholine. *Pflugers Arch.* **2004**, *447*, 636–640.
(6) Roghani, A.; Feldman, J.; Kohan, S. A.; Shirzadi, A.; Gundersen, C. B.; Brecha, N.; Edwards, R. H. Molecular cloning of a putative vesicular transporter for acetylcholine. *Proc. Natl. Acad. Sci. U.S.A.* **1994**, *91*, 10620–10624.
(7) Erickson, J. D.; Varoqui, H.; Schafer, M. K.; Modi, W.; Diebler, M. F.; Weihe, E.; Rand, J.; Eiden, L. E.; Bonner, T. I.; Usdin, T. B. Functional identification of a vesicular acetylcholine transporter and its expression from a "cholinergic" gene locus. *J. Biol. Chem.* **1994**, *269*, 21929–21932.
(8) Jensen, A. A.; Frolund, B.; Liljefors, T.; Krogsgaard-Larsen, P. Neuronal nicotinic acetylcholine receptors: Structural revelations, target identifications, and therapeutic inspirations. *J. Med. Chem.* **2005**, *48*, 4705–4745.
(9) Bando, K.; Taguchi, K.; Ginoza, Y.; Naganuma, T.; Tanaka, Y.; Koike, K.; Takatoku, K. Synthesis and evaluation of radiolabeled piperazine derivatives of vesamicol as SPECT agents for cholinergic neurons. *Nucl. Med. Biol.* **2001**, *28*, 251–260.
(10) Efange, S. M. N. In vivo imaging of the vesicular acetylcholine transporter and the vesicular monoamine transporter. *FASEB J.* **2000**, *14*, 2401–2413.
(11) Jung, Y. W.; Frey, K. A.; Mulholland, G. K.; del Rosario, R.; Sherman, P. S.; Raffel, D. M.; Van Dort, M. E.; Kuhl, D. E.; Gildersleeve, D. L.; Wieland, D. M. Vesamicol receptor mapping of brain cholinergic neurons with radioiodine-labeled positional isomers of benzovesamicol. *J. Med. Chem.* **1996**, *39*, 3331–3342.
(12) Coenen, H. H. Fluorine-18 labeling methods: Features and possibilities of basic reactions. *Ernst Schering Res. Found. Workshop* **2007**, *62*, 15–50.
(13) Efange, S. M.; Mach, R. H.; Smith, C. R.; Khare, A. B.; Foulon, C.; Akella, S. K.; Childers, S. R.; Parsons, S. M. Vesamicol analogues as sigma ligands. Molecular determinants of selectivity at the vesamicol receptor. *Biochem. Pharmacol.* **1995**, *49*, 791–797.
(14) Anderson, D. C.; King, S. C.; Parsons, S. M. Pharmacological characterization of the acetylcholine transport system in purified Torpedo electric organ synaptic vesicles. *Mol. Pharmacol.* **1983**, *24*, 48–54.
(15) Bahr, B. A.; Parsons, S. M. Demonstration of a receptor in Torpedo synaptic vesicles for the acetylcholine storage blocker L-*trans*-2-(4-phenyl[3,4-^3H]-piperidino) cyclohexanol. *Proc. Natl. Acad. Sci. U.S.A.* **1986**, *83*, 2267–2270.
(16) Altar, C. A.; Marien, M. R. [3H]Vesamicol binding in brain: Autoradiographic distribution, pharmacology, and effects of cholinergic lesions. *Synapse* **1988**, *2*, 486–493.
(17) Van der Kloot, W. Loading and recycling of synaptic vesicles in the Torpedo electric organ and the vertebrate neuromuscular junction. *Prog. Neurobiol.* **2003**, *71*, 269–303.
(18) Ishiwata, K.; Kawamura, K.; Yajima, K.; QuingGeLeTu; Mori, H.; Shiba, K. Evaluation of (+)-*p*-[^{11}C]methylvesamicol for mapping sigma1 receptors: A comparison with [^{11}C]SA4503. *Nucl. Med. Biol.* **2006**, *33*, 543–548.
(19) Kawamura, K.; Shiba, K.; Tsukada, H.; Nishiyama, S.; Mori, H.; Ishiwata, K. Synthesis and evaluation of vesamicol analog (−)-*O*-[^{11}C]methylvesamicol as a PET ligand for vesicular acetylcholine transporter. *Ann. Nucl. Med.* **2006**, *20*, 417–424.
(20) Shiba, K.; Ogawa, K.; Ishiwata, K.; Yajima, K.; Mori, H. Synthesis and binding affinities of methylvesamicol analogs for the acetylcholine transporter and sigma receptor. *Bioorg. Med. Chem.* **2006**, *14*, 2620–2626.

(21) Rogers, G. A.; Kornreich, W. D.; Hand, K.; Parsons, S. M. Kinetic and equilibrium characterization of vesamicol receptor−ligand complexes with picomolar dissociation constants. *Mol. Pharmacol.* **1993**, *44*, 633–641.
(22) Rogers, G. A.; Stone-Elander, S.; Ingvar, M.; Eriksson, L.; Parsons, S. M.; Widen, L. ^{18}F-Labelled vesamicol derivatives: Syntheses and preliminary in vivo small animal positron emission tomography evaluation. *Nucl. Med. Biol.* **1994**, *21*, 219–230.
(23) DeGrado, T. R.; Mulholland, G. K.; Wieland, D. M.; Schwaiger, M. Evaluation of (−)[^{18}F]fluoroethoxybenzovesamicol as a new PET tracer of cholinergic neurons of the heart. *Nucl. Med. Biol.* **1994**, *21*, 189–195.
(24) Mulholland, G. K.; Wieland, D. M.; Kilbourn, M. R.; Frey, K. A.; Sherman, P. S.; Carey, J. E.; Kuhl, D. E. [^{18}F]Fluoroethoxybenzovesamicol, a PET radiotracer for the vesicular acetylcholine transporter and cholinergic synapses. *Synapse* **1998**, *30*, 263–274.
(25) Jung, Y. W.; Van Dort, M. E.; Gildersleeve, D. L.; Wieland, D. M. A radiotracer for mapping cholinergic neurons of the brain. *J. Med. Chem.* **1990**, *33*, 2065–2068.
(26) Sorger, D.; Schliebs, R.; Kampfer, I.; Rossner, S.; Heinicke, J.; Dannenberg, C.; Georgi, P. In vivo [^{125}I]-iodobenzovesamicol binding reflects cortical cholinergic deficiency induced by specific immunolesion of rat basal forebrain cholinergic system. *Nucl. Med. Biol.* **2000**, *27*, 23–31.
(27) Mach, R. H.; Voytko, M. L.; Ehrenkaufer, R. L.; Nader, M. A.; Tobin, J. R.; Efange, S. M.; Parsons, S. M.; Gage, H. D.; Smith, C. R.; Morton, T. E. Imaging of cholinergic terminals using the radiotracer [^{18}F](+)-4-fluorobenzyltrozamicol: In vitro binding studies and positron emission tomography studies in nonhuman primates. *Synapse* **1997**, *25*, 368–380.
(28) Efange, S. M.; Mach, R. H.; Khare, A.; Michelson, R. H.; Nowak, P. A.; Evora, P. H. *p*-[^{18}F]Fluorobenzyltrozamicol ([^{18}F]FBT): Molecular decomposition-reconstitution approach to vesamicol receptor radioligands for positron emission tomography. *Appl. Radiat. Isot.* **1994**, *45*, 465–472.
(29) Gage, H. D.; Voytko, M. L.; Ehrenkaufer, R. L.; Tobin, J. R.; Efange, S. M.; Mach, R. H. Reproducibility of repeated measures of cholinergic terminal density using [^{18}F](+)-4-fluorobenzyltrozamicol and PET in the rhesus monkey brain. *J. Nucl. Med.* **2000**, *41*, 2069–2076.
(30) Voytko, M. L.; Mach, R. H.; Gage, H. D.; Ehrenkaufer, R. L.; Efange, S. M.; Tobin, J. R. Cholinergic activity of aged rhesus monkeys revealed by positron emission tomography. *Synapse* **2001**, *39*, 95–100.
(31) Efange, S. M.; Michelson, R. H.; Khare, A. B.; Thomas, J. R. Synthesis and tissue distribution of (*m*-[^{125}I]iodobenzyl)trozamicol ([^{125}I]MIBT): Potential radioligand for mapping central cholinergic innervation. *J. Med. Chem.* **1993**, *36*, 1754–1760.
(32) Staley, J. K.; Mash, D. C.; Parsons, S. M.; Khare, A. B.; Efange, S. M. Pharmacological characterization of the vesamicol analogue (+)-[^{125}I]MIBT in primate brain. *Eur. J. Pharmacol.* **1997**, *338*, 159–169.
(33) Efange, S. M.; Garland, E. M.; Staley, J. K.; Khare, A. B.; Mash, D. C. Vesicular acetylcholine transporter density and Alzheimer's disease. *Neurobiol. Aging* **1997**, *18*, 407–413.
(34) Kuhl, D. E.; Koeppe, R. A.; Fessler, J. A.; Minoshima, S.; Ackermann, R. J.; Carey, J. E.; Gildersleeve, D. L.; Frey, K. A.; Wieland, D. M. In vivo mapping of cholinergic neurons in the human brain using SPECT and IBVM. *J. Nucl. Med.* **1994**, *35*, 405–410.
(35) Kuhl, D. E.; Minoshima, S.; Fessler, J. A.; Frey, K. A.; Foster, N. L.; Ficaro, E. P.; Wieland, D. M.; Koeppe, R. A. In vivo mapping of cholinergic terminals in normal aging, Alzheimer's disease, and Parkinson's disease. *Ann. Neurol.* **1996**, *40*, 399–410.
(36) Widen, L.; Eriksson, M.; Ingvar, M.; Parsons, M.; Rogers, G. A.; Stone-Elander, S. PET studies of central cholinergic nerve terminals in animals and man. *J. Cereb. Blood Flow Metab.* **1993**, *13*, S300.
(37) Cramer, R. D., III; Patterson, D. E.; Bunce, J. D. Comparative molecular field analysis (CoMFA). 1. Effect of shape on binding of steroids to carrier proteins. *J. Am. Chem. Soc.* **1988**, *110*, 5959–5967.
(38) Kubinyi, H., Ed. 3D-QSAR in Drug Design. Theory, Methods and Applications; ESCOM: Leiden, The Netherlands, 1993.
(39) Efange, S. M.; von Hohenberg, K.; Khare, A. B.; Tu, Z.; Mach, R. H.; Parsons, S. M. Synthesis and biological characterization of stable and radioiodinated (±)-*trans*-2-hydroxy-3-P[4-(3-iodophenyl)piperidyl]-1,2,3,4-tetrahydronaphthalene (3′-IBVM). *Nucl. Med. Biol.* **2000**, *27*, 749–755.
(40) Efange, S. M.; Mach, R. H.; Smith, C. R.; Khare, A. B.; Foulon, C.; Akella, S. K.; Childers, S. R.; Parsons, S. M. Vesamicol analogues as sigma ligands. Molecular determinants of selectivity at the vesamicol receptor. *Biochem. Pharmacol.* **1995**, *49*, 791–797.
(41) Khare, A. B.; Langason, R. B.; Parsons, S. M.; Mach, R. H.; Efange, S. M. *N*-(3-Iodophenyl)trozamicol (IPHT) and related inhibitors of vesicular acetylcholine transport: Synthesis and preliminary biological characterization. *Nucl. Med. Biol.* **1999**, *26*, 609–617.
(42) Efange, S. M.; Khare, A. B.; Mach, R. H.; Parsons, S. M. Hydroxylated decahydroquinolines as ligands for the vesicular acetylcholine transporter: Synthesis and biological evaluation. *J. Med. Chem.* **1999**, *42*, 2862–2869.
(43) Efange, S. M.; Khare, A. B.; Foulon, C.; Akella, S. K.; Parsons, S. M. Spirovesamicols: Conformationally restricted analogs of 2-(4-phenylpiperidino)cyclohexanol (vesamicol, AH5183) as potential modulators of presynaptic cholinergic function. *J. Med. Chem.* **1994**, *37*, 2574–2582.
(44) Efange, S. M.; Kamath, A. P.; Khare, A. B.; Kung, M. P.; Mach, R. H.; Parsons, S. M. *N*-Hydroxyalkyl derivatives of 3-beta-phenyltropane and 1-methylspiro[1*H*-indoline-3,4′-piperidine]: Vesamicol analogues with affinity for monoamine transporters. *J. Med. Chem.* **1997**, *40*, 3905–3914.
(45) Wold, S.; Ruhe, A.; Wold, H.; Dunn, W. J. The collinearity problem in linear regression. The partial least-squares (PLS) approach to generalized inverses. *Siam J. Sci. Stat. Comp.* **1984**, *5*, 735–743.
(46) Cramer, R. D.; Bunce, J. D.; Patterson, D. E.; Frank, I. E. Cross-validation, bootstrapping, and partial least-squares compared with multiple-regression in conventional QSAR studies. *Quant. Struct.-Act. Rel.* **1988**, *7*, 18–25.
(47) *SYBYL 7.0*; Tripos Inc.: St. Louis, MO, 2004.
(48) Baroni, M.; Costantino, G.; Crucian, G.; Riganelli, D.; Valigi, R.; Clementi, S. Generating optimal linear PLS estimations (GOLPE): An advanced chemometric tool for handling 3D QSAR problems. *Quant. Struct.-Act. Relat.* **1993**, *12*, 9–20.
(49) Shao, J. Linear model selection by cross-validation. *J. Am. Stat. Assoc.* **1993**, *88*, 486–494.
(50) Boháč, M.; Loeprecht, B.; Damborský, J.; Schüürmann, G. Impact of orthogonal signal correction (OSC) on the predictive ability of CoMFA models for the ciliate toxicity of nitrobenzenes. *Quant. Struct.-Act. Relat.* **2002**, *21*, 3–11.
(51) Salama, I.; Hocke, C.; Utz, W.; Prante, O.; Boeckler, F.; Hübner, H.; Kuwert, T.; Gmeiner, P. Structure-selectivity investigations of D_2-like receptor ligands by CoMFA and CoMSIA guiding the discovery of D_3 selective PET radioligands. *J. Med. Chem.* **2007**, *50*, 489–500.
(52) Sadowski, J.; Gasteiger, J. From atoms and bonds to three-dimensional atomic coordinates: Automatic model builders. *Chem. Rev.* **1993**, *93*, 2567–2581.

JM700961R